Skin sodium is increased in male patients with multiple sclerosis and related animal models

Konstantin Huhn[a,1], Peter Linz[b,1], Franziska Pemsel[a,c], Bernhard Michalke[d], Stefan Seyferth[e], Christoph Kopp[f], Mohammad Anwar Chaudri[g,2], Veit Rothhammer[a], Arnd Dörfler[h], Michael Uder[b], Armin M. Nagel[b,i], Dominik N. Müller[j,k,l], Anne Waschbisch[a,3], De-Hyung Lee[m], Tobias Bäuerle[b], Ralf A. Linker[m], and Stefanie Haase[m,4]

[a]Department of Neurology, Friedrich–Alexander University Erlangen–Nuremberg, 91054 Erlangen, Germany; [b]Department of Radiology, Friedrich–Alexander University Erlangen–Nuremberg, 91054 Erlangen, Germany; [c]Department of Radiation Therapy, University Hospital Würzburg, 97080 Würzburg, Germany; [d]Research Unit Analytical BioGeoChemistry, Helmholtz Zentrum München German Research Center for Environmental Health, 85764 Munich, Germany; [e]Division of Pharmaceutics, Friedrich–Alexander University Erlangen–Nuremberg, 91054 Erlangen, Germany; [f]Department of Nephrology and Hypertension, University Hospital Erlangen, 91054 Erlangen, Germany; [g]Institute of Corrosion and Surface Science, Department of Material Science, Friedrich–Alexander University Erlangen–Nuremberg, 91054 Erlangen, Germany; [h]Department of Neuroradiology, University Hospital Erlangen, Friedrich–Alexander University Erlangen–Nuremberg, 91054 Erlangen, Germany; [i]Division of Medical Physics in Radiology, German Cancer Research Center, 69120 Heidelberg, Germany; [j]Experimental and Clinical Research Center, Max Delbrück Center for Molecular Medicine and Charité-Universitätsmedizin, 13125 Berlin, Germany; [k]Max Delbrück Center for Molecular Medicine in the Helmholtz Association, 13125 Berlin, Germany; [l]Berlin Institute of Health, 13125 Berlin, Germany; and [m]Department of Neurology, University Hospital Regensburg, 93053 Regensburg, Germany

Edited by Lawrence Steinman, Stanford University School of Medicine, Stanford, CA, and approved May 20, 2021 (received for review February 8, 2021)

Novel MRI techniques allow a noninvasive quantification of tissue sodium and reveal the skin as a prominent compartment of sodium storage in health and disease. Since multiple sclerosis (MS) immunopathology is initiated in the periphery and increased sodium concentrations induce proinflammatory immune cells, the skin represents a promising compartment linking high sodium concentrations and MS immunopathology. We used a 7-T sodium MRI (^{23}Na-MRI) and inductively coupled plasma mass spectrometry to investigate the skin sodium content in two mouse models of MS. We additionally performed 3-T ^{23}Na-MRI of calf skin and muscles in 29 male relapsing-remitting MS (RRMS) patients and 29 matched healthy controls. Demographic and clinical information was collected from interviews, and disease activity was assessed by expanded disability status scale scoring. ^{23}Na-MRI and chemical analysis demonstrated a significantly increased sodium content in the skin during experimental autoimmune encephalomyelitis independent of active immunization. In male patients with RRMS, ^{23}Na-MRI demonstrated a higher sodium signal in the area of the skin compared to age- and biological sex-matched healthy controls with higher sodium, predicting future disease activity in cranial MRI. In both studies, the sodium enrichment was specific to the skin, as we found no alterations of sodium signals in the muscle or other tissues. Our data add to the recently identified importance of the skin as a storage compartment of sodium and may further represent an important organ for future investigations on salt as a proinflammatory agent driving autoimmune neuroinflammation such as that in MS.

multiple sclerosis | sodium magnetic resonance imaging | skin | experimental autoimmune encephalomyelitis

Multiple sclerosis (MS) is a chronic autoimmune inflammatory disease of the central nervous system (CNS). Despite considerable research effort, its detailed pathogenesis remains to be elucidated. Among others, environmental and nutritional factors are discussed to impact MS etiology, and recently, salt and sodium turned into the focus of research. Recent studies demonstrated that high sodium concentrations increase the differentiation of murine and human T helper 17 (Th17) cells and induce a highly pathogenic phenotype (1, 2). In the model disease experimental autoimmune encephalomyelitis (EAE), high sodium chloride intake augmented disease onset and severity accompanied by the induction of proinflammatory macrophages (3, 4) and an increased infiltration of Th17 cells in the spinal cord (1, 2, 5). Moreover, high sodium concentrations also activate human monocytes, thus leading to an increased capacity to induce IL-17A production in human T cells (6). First, clinical trials in MS revealed that increased dietary sodium intake is accompanied by enhanced disease activity, relapse risk, and an increased MRI signal (7). Yet, follow-up studies in adult and pediatric MS did not demonstrate a positive correlation between MS and high salt intake (8–11). All studies used food-frequency questionnaires and spot urine samples to estimate the sodium intake of study participants. However, the assumption that an increased sodium intake directly correlates with sodium excretion has recently been challenged (12). Long-term studies investigating sodium intake and excretion revealed that large amounts of sodium accumulate in the body without commensurate water retention (13–16). Sodium was shown to accumulate in the muscle and the skin interstitium in abundance over water, creating a local electrolyte environment that does not equilibrate with plasma and hence escapes control of the kidney (17–20). Instead, this skin sodium storage was shown to rely on extrarenal regulatory mechanisms involving the immune system (18, 21). This finding prompted many researchers to investigate a potential contribution of tissue-sodium storage in various

Significance

Our data add to the recently identified importance of the skin as a storage compartment of sodium. We found a higher sodium MRI (^{23}Na-MRI) signal in the skin of male multiple sclerosis (MS) patients compared to matched healthy controls as well as in the animal model, experimental autoimmune encephalomyelitis. Considering the salt effects on macrophage and T-cell immunology during MS and the persisting challenge to accurately determine the actual sodium load via salt excretion, the noninvasive determination of sodium by ^{23}Na-MRI analysis of the skin may represent an important method for further investigations on sodium and MS risk.

Author contributions: K.H., P.L., R.A.L., and S.H. designed research; K.H., P.L., F.P., B.M., S.S., C.K., M.A.C., A.M.N., A.W., D.-H.L., T.B., and S.H. performed research; K.H., P.L., F.P., B.M., S.S., C.K., M.A.C., V.R., A.D., M.U., A.M.N., D.N.M., A.W., D.-H.L., T.B., and S.H. analyzed data; and K.H., R.A.L., and S.H. wrote the paper.

The authors declare no competing interest.

This article is a PNAS Direct Submission.

Published under the PNAS license.

See online for related content such as Commentaries.

[1]K.H. and P.L. contributed equally to this work.

[2]Deceased November 11, 2017.

[3]Present address: Department of Neurology, University Rheinisch-Westfälische Technische Hochschule (RWTH) Aachen, 52062 Aachen, Germany.

[4]To whom correspondence may be addressed. Email: stefanie.haase@ukr.de.

Published July 6, 2021.

Downloaded at Palestinian Territory, occupied on November 29, 2021

www.manaraa.com

diseases. First, studies identified a higher skin sodium content in patients with arterial hypertension (22, 23), systemic sclerosis (24), and bacterial skin infections (25). Later, higher sodium content in muscle and skin was also detected in patients with type 2 diabetes (26, 27), systemic lupus erythematosus (28), acute and chronic heart failure (29), and chronic kidney disease (30–32). All studies used sodium (^{23}Na)-MRI, which allows a direct, noninvasive measurement of tissue-sodium concentrations. In MS, in vivo ^{23}Na-MRI has already been performed on brain tissue, identifying an increased brain sodium accumulation already in early beginning relapsing-remitting MS (RRMS) (33–35). Yet, the inflammatory pathogenesis of MS is assumed to be initiated in the periphery. Considering the salt effects on macrophage and T-cell immunology during MS and the persisting challenge to accurately determine salt intake via salt excretion, the skin may represent an important organ for further investigations on sodium and MS risk. We thus investigated the skin sodium content during neuroinflammation in two mouse models of MS and in 29 male RRMS patients and healthy controls (HC) by noninvasive ^{23}Na-MRI and chemical analysis.

Results

Skin Sodium Content Is Increased in Mouse Models of MS. We employed noninvasive 7-T ^{23}Na-MRI to analyze the ^{23}Na-MRI signal in the area of the skin during myelin oligodendrocyte glycoprotein–induced EAE (MOG-EAE) as a prototype model of neuroinflammation. We analyzed male mice at the maximum of MOG-EAE (day 16 after immunization) compared to nonimmunized naïve control mice with similar mean age (EAE: 13.2 ± 0.5 wk; naïve: 13.5 ± 0.3 wk) and mean body weight (EAE: 21.5 ± 3.6 g; naïve: 22.3 ± 2.8 g). EAE-diseased mice suffered from a mild paraparesis with a mean clinical EAE score of 2.8 ± 0.52 and showed no signs of abnormal self-preservation behaviors. Estimation of skin sodium by relating the signal intensity to known concentrations in a linear trend analysis revealed significantly higher sodium-signal intensities in EAE-diseased mice compared to naïve controls (Fig. 1 *A* and *B*). To confirm our ^{23}Na-MRI data, we further performed chemical analysis of the sodium content in different organs from these mice. Inductively coupled plasma mass spectrometry (ICP-AES) of freeze-dried skin tissue revealed a significantly higher sodium content in mice on the maximum of EAE compared to naïve controls (Fig. 2*A*). Additional ICP-AES analysis of mice on days 3 and 9 after MOG-EAE induction revealed a sodium enrichment in the skin already at the beginning of the disease, but this was only significant on day 16 of EAE (Fig. 2*A*). The sodium enrichment was specific to the skin, as there was no effect in various other tissues including the spleen, the spinal cord, the kidneys, and the gut (Fig. 2 *B–E*). Similarly, the enrichment in the skin was specific for sodium, since we found no altered potassium content in the skin or in any other tissues after EAE induction compared to naïve control mice (Fig. 2 *F–J*). To exclude any unspecific effects of local inflammation at the immunization site, we analyzed the skin sodium content in a transgenic mouse model of neuroinflammation that is independent from subcutaneous injection. Age- (12.8 ± 2.6 wk) and biological sex- (male) matched MOG-transgenic 2D2 mice showed a significantly higher sodium content in the skin compared to naïve control mice (Fig. 2*K*). Thus, we found a significant sodium enrichment specifically in the skin during experimental neuroinflammation that is independent from active immunization or mediated by local inflammation.

^{23}Na-MRI Signal in the Area of the Skin Is Increased in Patients with RRMS. We next investigated the clinical relevance of the ^{23}Na-MRI signal in the area of the skin during neuroinflammation by analyzing male and female patients with RRMS and age- and biological sex-matched HC. ^{23}Na-MRI revealed no differences in the sodium signal in the skin of female RRMS patients compared to female, age-matched HC (MS: 15.19 ± 3.32 a.u.; HC: 13.31 ± 1.55 a.u.; $n = 8$ per group; $P = 0.1028$ by unpaired Student's t test). Yet, female participants showed significantly lower sodium signals in the skin compared to the male group, confirming recently published data that demonstrated a potential bias by biological sex and hormone status (23, 36). We thus focused our study on male subjects and analyzed 29 male patients with RRMS and 29 male, age-matched HC. Study participants displayed a mean age of 31.9 y in MS and 31.2 y in HC with a similar mean body weight (MS: 81.8 kg; HC: 79.2 kg), body mass index (BMI) (MS: 24.8 kg/m^2; HC: 23.5 kg/m^2), body fat (MS: 25.2%; HC 21.7%), and total body water percentage (MS: 43.5%; HC: 43.9%). Routine blood-pressure investigation excluded marked hypertension in all individuals. Mean serum levels for sodium (MS: 141.3 mmol/L; HC: 140.8 mmol/L) and potassium (MS: 4.2 mmol/L; HC: 3.9 mmol/L) were in the normal range and did not differ significantly between the two groups, and neither did the levels of further routine serum markers or blood-cell counts (Table 1). RRMS patients had a mean disease duration of 5.5 y after diagnosis was established (Table 2). Disease severity was mild as displayed by a median expanded disability status scale (EDSS) score of 1.5 (interquartile range: 1.0 to 3.0). Immunomodulatory treatment of the RRMS patients at the time of investigation comprised oral therapies (fingolimod $n = 8$; dimethyl fumarate $n = 4$), monoclonal antibodies (natalizumab $n = 5$; ocrelizumab $n = 4$), and injectables (beta interferons $n = 4$; glatiramer acetate $n = 3$). One MS patient was not treated (therapy naïve) at the time point of analysis. For patients treated with injectables, any previous (mis)application within or near the calf area was excluded prior to ^{23}Na-MRI investigation of this region. Our ^{23}Na-MRI investigations of the respective calf regions revealed a higher ^{23}Na-MRI signal in the area of the skin of male RRMS versus HC (Fig. 3 *A* and *B*). To avoid a potential bias of sodium levels due to age (19, 23), we additionally performed an age-matched paired analysis that also demonstrated

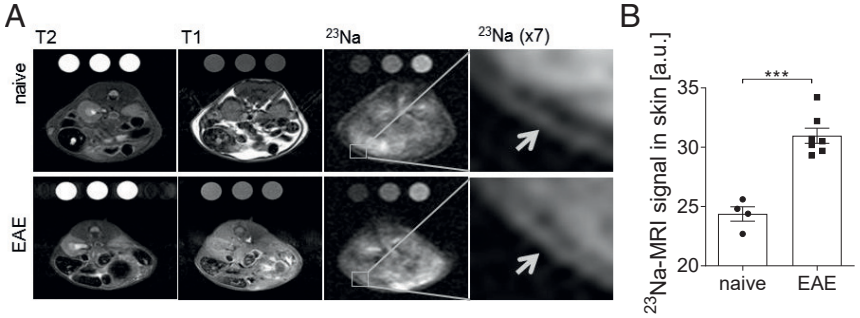

Fig. 1. ^{23}Na-MRI reveals an increased sodium signal in the area of the skin in mouse models of MS. (*A* and *B*) The ^{23}Na-MRI signal in the area of the skin of naïve control mice and mice on day 16 of EAE was analyzed by 7-T ^{23}Na-MRI. (*A*) Representative anatomic images (T2- and T1-weighted) and sodium (^{23}Na) images of age- and biological sex-matched mice. (*B*) Quantification of total sodium content in the skin of naïve control mice and mice on day 16 of EAE (naïve $n = 4$, EAE $n = 7$ from two independent measurements). Data are given as mean ± SEM. ***$P < 0.001$ by unpaired two-tailed Student's t test.

Downloaded at Palestinian Territory, occupied on November 29, 2021
www.manaraa.com

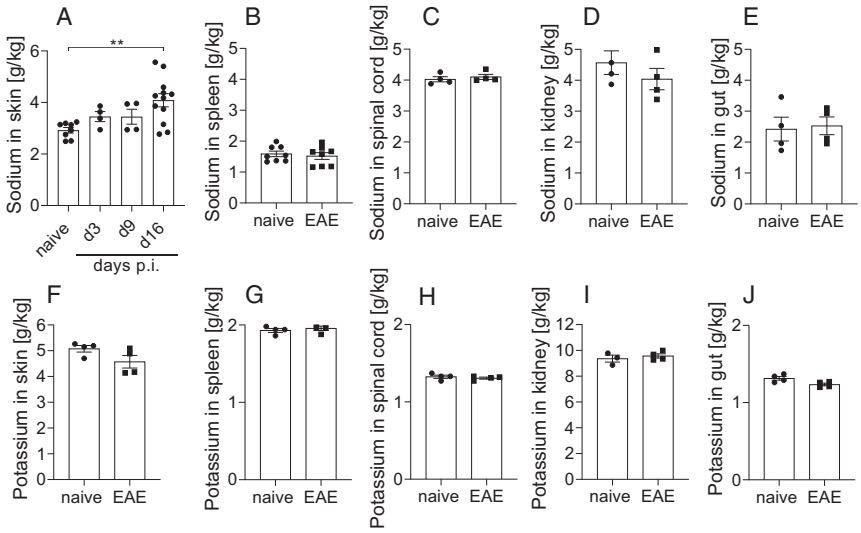

Fig. 2. Chemical analysis confirms the skin-specific sodium increase during neuroinflammation. (*A*) Sodium content in the skin was analyzed by ICP-AES of ashed tissue sampled from naïve control mice and mice on day 3, day 9, and day 16 of EAE (naïve $n = 8$ from two independent experiments, day 3 and day 9 $n = 4$, day 16 $n = 12$ from two independent experiments). (*B–E*) ICP-AES analysis of sodium concentrations in (*B*) the spleen, (*C*) the spinal cord, (*D*) the kidneys, and (*E*) the gut of naïve control mice and mice on day 16 of EAE (spleen $n = 8$ from two independent experiments, other tissues $n = 4$). (*F–J*) ICP-AES analysis of potassium concentrations in (*F*) the skin, (*G*) the spleen, (*H*) the spinal cord, (*I*) the kidneys, and (*J*) the gut of naïve control mice and mice on day 16 of EAE ($n = 4$ per group and tissue). (*K*) ICP-AES analysis of the skin sodium content in naïve control mice compared to MOG-transgenic 2D2 mice (naïve $n = 8$, 2D2 $n = 9$ from two independent experiments). Data are given as mean ± SEM. $^{**}P < 0.01$ by one-way ANOVA in *A*. p.i., post immunization.

a significantly higher sodium signal in MS patients compared to the controls (Fig. 3*C*). In contrast, the ^{23}Na-MRI signal was not elevated in the respective calf muscles (i.e., musculus triceps surae, Fig. 3*D*) or the tibial bone marrow (Fig. 3*E*). We further applied a proton (^{1}H) fat–saturated inversion-recovery sequence and a trend analysis relative to the 10-mM aqueous phantom flask. We found an increased ^{1}H fat–saturated signal in the area of the skin of MS patients (Fig. 3*F*) that was spared in muscle or bone tissue of MS patients (Fig. 3 *G* and *H*). Yet, bioimpedance spectroscopy measurements revealed no excess extracellular water (overhydration) in MS patients compared to age-matched controls (Fig. 3*I*). Moreover, differences in skin thickness as a potential confounder of sodium levels were excluded, as mean thickness measured by MRI was 1.35 ± 0.19 mm for both groups. We additionally analyzed the routine MRI follow-up data in MS patients. According to the mean ^{23}Na-MRI signal in the skin, we divided MS patients into "Na-high" (>18.0 a.u.) and "Na-low" (≤18.0 a.u.) groups and correlated these data to the numbers of patients showing MRI activity (a contrast of enhancing lesions or new or enlarging T2 lesions) within a mean follow-up period of 3.5 ± 2.1 y. While only 30% (3 out of 10) of MS patients with a low sodium signal in the skin showed MRI activity during the follow-up, 66% (6 out of 9) of MS patients with a high sodium signal displayed MRI activity (odds ratio [OR] = 4.66, Fig 3*J*). These data lend further credit to a potential association of skin sodium content with future disease activity.

Discussion

Our noninvasive ^{23}Na-MRI measurements revealed a higher ^{23}Na-MRI signal in the area of the skin during experimental neuroinflammation and in male patients with RRMS, suggesting a selective enrichment of sodium in the skin during neuroinflammation. The murine data were additionally confirmed by direct tissue-sodium measurement using ICP-AES. This method revealed no alterations of the sodium content in the gut, the spleen, or the kidneys as relevant immune organs or the spinal cord as a target organ during neuroinflammation. Adding to this, we found no alterations of the sodium content in human MRI of the calf muscle or tibial bone marrow, thus arguing for a skin-specific sodium accumulation during neuroinflammation. By using 2D2 mice, we also excluded the possibility that any skin effect during neuroinflammation was governed by local inflammation at the immunization site. Moreover, factors that were already shown to influence skin sodium content, such as age (19, 23), weight, biological sex (23, 36), or aldosterone (22), were carefully controlled by analyzing age- and gender-matched individuals in both the murine and the human study as well as by excluding relevant comorbidities. For human MRI, we further

Table 1. Baseline parameters of male RRMS patients and HC for the ^{23}Na-MRI analysis in Fig. 3

Parameters	Healthy controls	MS
Age (years)	31.2 ± 6.5	31.9 ± 5.9
Weight (kg)	79.2 ± 14.2	81.8 ± 11.6
BMI (kg/m^2)	23.5 ± 4.2	24.8 ± 3.5
Body fat (%)	21.7 ± 7.7	25.2 ± 7.3
Body water (%)	43.9 ± 5.6	43.5 ± 4.1
Overhydration (L)	0.45 ± 1.13	0.44 ± 1.27
Na (mmol/L)	140.8 ± 1.6	141.3 ± 1.9
K (mmol/L)	3.9 ± 0.5	4.2 ± 0.5
Creatinine (mg/dL)	0.9 ± 0.1	0.9 ± 0.1
SBP (mmHg)	123.3 ± 10.9	127.9 ± 8.3
DBP (mmHg)	74.8 ± 5.3	76.2 ± 5.9
CRP (mg/dL)	1.4 ± 0.9	2.1 ± 5.4
LDH (U/L)	278.5 ± 62.3	260.1 ± 47.3
Leukocytes × 10^3/μL	6.7 ± 1.5	6.6 ± 1.9
Erythrocytes × 10^6/μL	5.0 ± 0.2	5.1 ± 0.3
Thrombocytes × 10^3/μL	244.8 ± 31.0	239.7 ± 52.9
Hb (g/dL)	15.4 ± 0.9	15.2 ± 0.9
Hct (%)	45.4 ± 2.1	43.6 ± 7.7
MCH (pg)	30.5 ± 1.6	30.2 ± 1.3
MCHC (g/dL)	34.0 ± 1.0	33.9 ± 1.1
MCV (fl)	89.6 ± 4.3	89.2 ± 2.6

All data are shown as mean ± SD. Differences were not significant between HC and MS patients. SBP, systolic blood pressure; DBP, diastolic blood pressure; CRP, C-reactive protein; LDH, lactate dehydrogenase; Hb, hemoglobin; Hct, hematocrit; MCH, mean corpuscular hemoglobin; MCHC, concentration; MCV, volume.

Downloaded at Palestinian Territory, occupied on November 29, 2021

www.manaraa.com

Table 2. Disease characteristics of male RRMS patients

Parameters	MS patient
EDSS (median [interquartile range])	1.5 (1.0 to 3.0)
Disease duration (median [interquartile range])	4.0 (2.0 to 8.0)
Disease duration (years)	5.5 ± 5.9
Fingolimod-treated (*n*)	8
Natalizumab-treated (*n*)	5
Ocrelizumab-treated (*n*)	4
Beta-interferone–treated (*n*)	4
Dimethyl fumerate–treated (*n*)	4
Glatiramer acetate–treated (n)	3
Therapy naïve (n)	1

restricted our investigation to subjects with Caucasian origin, as effects of different ethnicities and/or skin thickness could not be excluded (37). Moreover, we performed ^{23}Na-MRI analysis on male and female MS patients and HC. As known from previous ^{23}Na-MRI studies, we could detect a higher sodium signal in males than in females (19, 23). In MS, male MS patients displayed a significantly higher sodium signal in the area of the skin compared to age-matched HC, while the skin sodium signal was comparable in female MS patients and matched controls.

As a limitation of skin ^{23}Na-MRI measurements, depending on the cutaneous architecture, diagnostic accuracy is compromised by partial volume effects. However, to obtain comparable sodium measurements, we employed the same settings in all measurements with careful positioning (19, 22, 23). Hence, these effects should be identical for different measurements. Moreover, using dedicated surface coils at ultrahigh magnetic-field strengths would achieve a higher spatial resolution (19), a method that will be applied for future studies. Yet, the study has some limitations. We identified a higher signal in ^{1}H fat–saturated inversion-recovery MRI in the skin of RRMS patients compared to HC, potentially caused by edema in the analyzed region. Subcutaneous edema represents a potential bias of the measured ^{23}Na-MRI signal of the skin, a fact that needs to be proven in future studies. However, the studied RRMS patients showed low EDSS scores without restriction in gait or obvious edema, contradicting the fact that edema of the lower limbs in MS patients has only been associated with a higher EDSS score, longer disease duration, and a chronic disease course (38). Furthermore, before the inclusion of MS patients, comorbidities or medication potentially compromising sodium or water balance were carefully excluded. Moreover, we additionally performed bioimpedance spectroscopy measurements of all investigated patients and HC to assess body water distribution. Bioimpedance spectroscopy revealed no difference in excess extracellular water (overhydration) between MS patients and HC, indicating that the increased skin Na^+ MRI signal in MS patients was not due to a general hypervolemia but may rather be governed by more complex changes in skin architecture, like lymph vessels.

Because of the observational nature of our study, any causal relationship between sodium stores and MS risk can only be hypothesized. Longitudinal studies are required to determine whether increased sodium content in skin precedes the development of MS or is a consequence of the disease. Moreover, the study comprises a small number of participants, and patients showed a mild form of RRMS. Thus, we cannot conclude that the skin sodium content would be also increased in severe RRMS or progressive forms of the disease. However, the low EDSS scores also exclude pronounced motor disabilities in the investigated cohort, thus excluding the possibility that the increased ^{23}Na-MRI signal in the calf skin is due to atrophy or immobility of the legs. Moreover, our data add to the important finding that sodium can be stored in the body and that a correlation between salt content and disease risk via sodium-excretion analysis or food-frequency questionnaires is oversimplified. This has already been discussed by other researchers, showing that ordinary urinary sodium analyses and nutritional questionnaires do not necessarily correspond to the actual sodium load (39–42). A first analysis in MS patients pointed at a correlation of increased dietary sodium intake with enhanced disease activity, relapse risk, and ^{23}Na-MRI signal intensity (7). However, follow-up studies in larger cohorts suggested no correlation between salt intake and MS (8–11). These opposing results may be related to the technique of sodium measurement rather than excluding salt as a potential risk factor for MS. ^{23}Na-MRI enables the visualization of the actual sodium content in the body, thus representing a more accurate method to determine the actual sodium load during health and disease compared to food questionnaires or sodium-excretion analysis. As mentioned in the Introduction, the use of ^{23}Na-MRI is gaining increasing importance and has been implemented in several studies (reviewed in refs. 43–45). For instance, an increased ^{23}Na-MRI signal has been identified in patients with arterial hypertension (22, 23), systemic sclerosis (24), and bacterial skin infections (25). Later, elevated ^{23}Na-MRI signals in muscle and skin were also detected in patients with type 2 diabetes (26, 27), systemic lupus erythematosus (28), acute and chronic heart failure (29), and chronic kidney disease (30–32). This study identifies an increased ^{23}Na-MRI signal in the skin of MS patients, potentially identifying an increased skin sodium content during neuroinflammation. Whether these increased salt concentrations in the skin are directly linked to the immunopathology of MS remains to be elucidated. Yet, analysis of routine MRI follow-up data in our cohort of MS patients lends further credit to a potential association of the skin sodium content with future disease activity in male patients. However, a larger cohort of MS patients would be necessary to further prove this observation. Considering the salt effects on macrophage and T-cell immunology (1–4, 6, 46, 47) and the persisting challenge to accurately determine the salt load via salt excretion, the skin may represent an important organ for further investigations on salt and MS risk. Interestingly, studies in patients with heart failure suggest that removal of skin sodium is possible with appropriate diuretic therapy (29). Whether diuretic treatment can decrease the skin sodium content during neuroinflammation and might thus represent a potential therapeutic option in MS needs to be proven in future studies.

Materials and Methods

Study Approval. All animal experiments were in accordance with the German laws for animal protection and were approved by the local ethic committees (Erlangen AZ 54-2532.1-56/12). Human studies were approved by the appropriate institutional review board at the Friedrich-Alexander-University Erlangen–Nuremberg according to the principles of the Declaration of Helsinki (approval no.: 136_14B). All participants gave their written informed consent.

Animal Experiments. C57BL/6J mice were initially purchased from Charles River Laboratories; mice harboring a transgenic MOG-specific T-cell receptor (2D2 mice) were a kind gift from Vijay Kuchroo, Harvard Medical School, Boston, MA. All mice were bred and housed at the Franz-Penzoldt-Zentrum, the animal care facility of the University of Erlangen–Nuremberg, under a 12-h day–night cycle and standardized environmental conditions, receiving normal chow (SNIFF E15431-34EF R/M) and tap water ad libitum. For EAE, a power calculation was performed (G*Power Freeware, version 3.1.5). For EAE induction, 10- to 12-wk-old male mice were anesthetized and subcutaneously injected with 200 μg MOG_{35-55} and 200 μg Freund's complete adjuvant (CFA). Pertussis toxin (200 ng per mouse) was applied intraperitoneally on days 0 and 2 after immunization. Clinical symptoms were assessed daily according to a five-point scale ranging from 0 (no symptoms) to 5 [moribund (1)].

Human Study Parameters. We included 29 healthy male subjects and 29 male patients (Table 1) suffering from RRMS after institutional review board approval according to the principles of the Declaration of Helsinki. We analyzed individually age- and biological sex-matched pairs of RRMS patients and controls to perform pairwise analysis. To avoid the potential influence

Downloaded at Palestinian Territory, occupied on November 29, 2021
www.manaraa.com

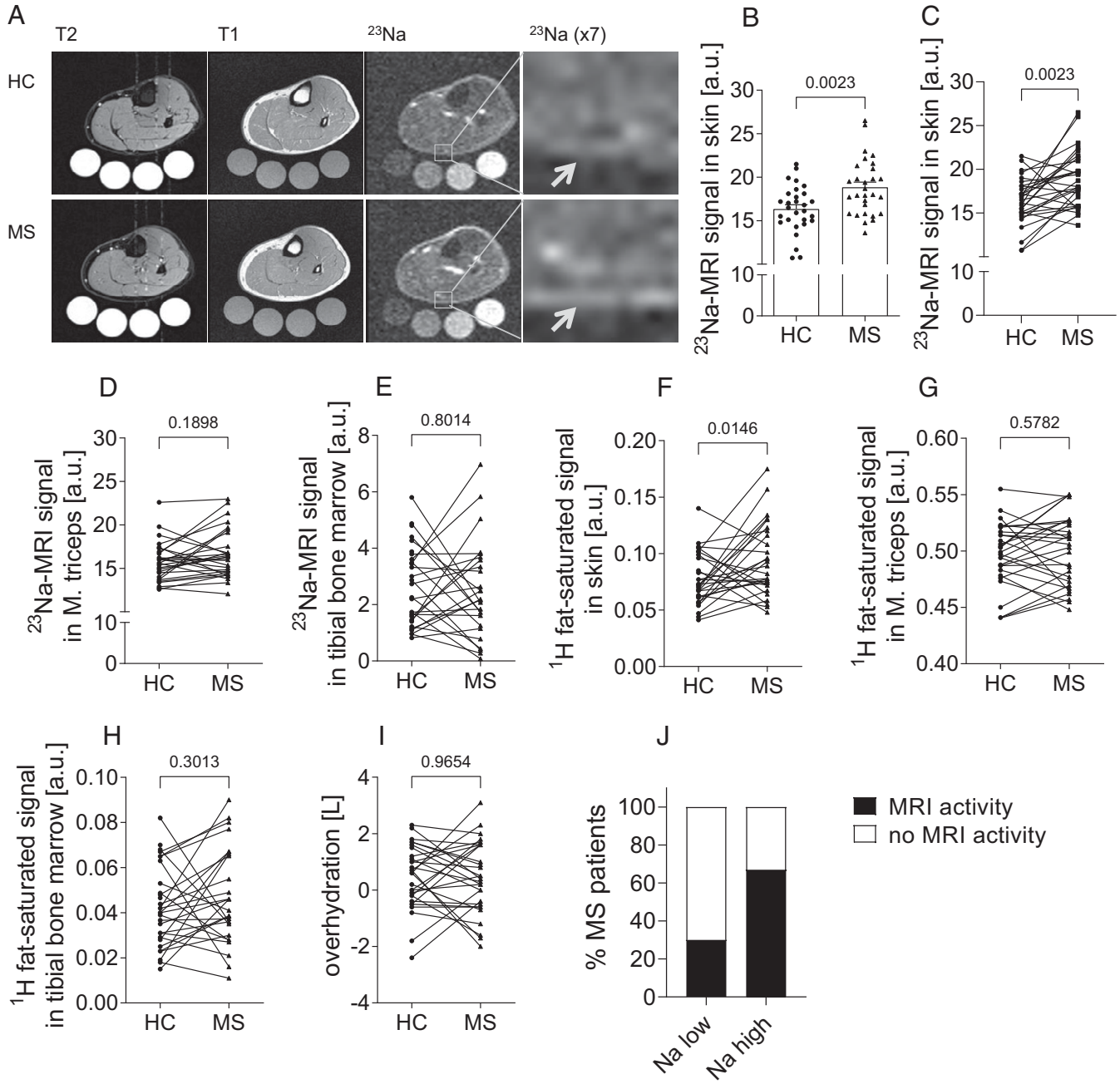

Fig. 3. ^{23}Na-MRI signal intensity in the area of the skin is increased in patients with RRMS. The ^{23}Na-MRI signal intensity in the area of the skin was analyzed in MS patients and age-, weight-, and biological sex-matched HC ($n = 29$ per group). The lower leg was positioned inside a 3-T ^{23}Na-MRI with a specific sodium coil. Four tubes containing aqueous solutions with increasing sodium concentrations (10, 20, 30, and 40 mM) were placed inside the coil and were used for normalization of the ^{23}Na-MRI signal intensities. (*A*) Representative T2 images, anatomic images (T1-weighted), and sodium (^{23}Na) images of matched individuals. Arrows in the pictures on the right indicate the sodium content in the skin in pictures with sevenfold magnification. (*B*) Quantification of total sodium in the skin. (*C*) Age-matched analysis of total sodium in the skin. (*D* and *E*) Quantification of total sodium in (*D*) musculus triceps surae and (*E*) the tibial bone marrow in age-matched MS patients and HC. (*F–H*) ^{1}H fat–saturated inversion-recovery signal in the (*F*) skin, (*G*) musculus triceps, and (*H*) tibial bone marrow of MS patients compared to age-matched HC. (*I*) Bioimpedance spectroscopy measurements of extracellular water (overhydration) in age-matched MS patients and HC. (*J*) Correlation between the skin sodium signal in MS patients and the percentage of MRI activity during a follow-up period of 3.5 ± 2.1 y. All data are given as mean ± SEM and were analyzed by unpaired two-tailed Student's *t* test.

of hormone status or intake of oral contraception, we predominantly investigated male participants. However, a smaller female cohort was also included to analyze for expected sex differences in sodium signal (19, 23). All participants gave their written informed consent. Only Caucasian participants were included in this study, as ethnicity could influence tissue-sodium levels (37). Exclusion criteria further comprised potential influencers of sodium or water balance (i.e., diagnosed hypertension, acute or chronic heart or kidney disease), intake of medication potentially influencing blood/tissue sodium (i.e., diuretics, antihypertensive drugs, carbamazepine, antibiotics, supplementation with electrolytes, or glucocorticoid therapy within the last 6 wk), progressive courses of MS, gait restriction (EDSS > 4.0), systemic or cutaneous autoimmune disease other than MS, obvious edema of the lower limbs, chronic or acute skin alterations, and previous trauma or injury of the tibial or calf region as well as intense sporting activity within the last 48 h. For MS patients receiving injectable immunomodulatory therapies, subcutaneous application within the respective calf area had to be excluded prior

Downloaded at Palestinian Territory, occupied on November 29, 2021

www.manaraa.com

to ^{23}Na-MRI. Clinical data and data of previous routine MRI scans of the CNS were acquired by review of medical charts and clinical investigation at presentation for ^{23}Na-MRI. Additionally, height, weight, and BMI were measured, and peripheral venous blood samples were taken for analysis of routine blood levels. Blood-pressure measurements were performed before ^{23}Na-MRI and were the average of three consecutive measurements and one after 15 min of rest for each participant. Body water distribution for each subject was assessed by bioimpedance spectroscopy (body composition monitor, Fresenius Medical Care) as described previously (26).

MRI Measurements in Humans. ^{23}Na-MRI was performed in transversal slices of the lower legs with a 3.0-T clinical MRI system (Verio, Siemens Healthcare) using a gradient echo sequence with acquisition time (TA) 13.7 min, echo time (TE) 2.07 ms, repetition time (TR) 100 ms, flip angle (FA) 90°, 128 averages, resolution: $3 \times 3 \times 30$ mm^3, and a frequency-adapted monoresonant transmit/receive birdcage knee coil (32.602 MHz, Stark Contrast). A ^{1}H fat–suppressed inversion-recovery sequence (TA: 6.22 min, inversion time: 210 ms, TE: 12 ms, TR: 3 s, FA1/2: 90°/180°, resolution: $1.5 \times 1.5 \times 5$ mm^3) and a ^{1}H T1–weighted fast low-angle shot (FLASH) sequence were acquired to assess anatomical details of the lower leg (TA: 2.08 min, TE: 2.46 ms, TR: 250 ms, FA: 60°, resolution: $0.75 \times 0.75 \times 5$ mm^3). Aqueous standard solutions with increasing NaCl concentrations (10, 20, 30, and 40 mM) served for the calibration of relative tissue Na^+ by a linear trend analysis.

MRI Measurements in Mice. The human MRI setup was translated to a 7.0-T ClinScan (Bruker) with a double-resonant ^{23}Na/^{1}H circular polarized transmit/receive birdcage coil (79.467 MHz, Stark Contrast) adapted for mice. Skin tissue was assessed in the abdominal region together with aqueous salt solutions containing 20, 40, and 60 mM NaCl. A T1-weighted spin-echo sequence (TA: 7.39 min, TE: 9 ms, TR: 2.1 s, FA: 90°, resolution: $0.125 \times 0.125 \times 1$ mm^3) and a T2-weighted turbo spin-echo sequence (TA 1.14 min, TE: 56 ms, TR: 3.3 s, FA: 140°, resolution: $0.125 \times 0.125 \times 1$ mm^3) were acquired for anatomical details. Na^+ concentrations were estimated similarly to the human scans using a gradient echo sequence: TA: 10.40 min, TE: 1.83 ms, TR: 20 ms, FA: 50°, resolution: $1 \times 1 \times 10$ mm^3.

Data Evaluation of ^{23}Na-MRI Analysis. Images of human individuals and mice were processed and analyzed by the public-domain program ImageJ. Regions of interest in the skin were defined where the calf (human MRI) or the abdominal region (murine MRI) was in direct contact with the cylindrical surface of the phantom holder. A threshold of twice the background noise defined the border of the skin, and a layer thickness of one pixel was evaluated. Grayscale measurements included aqueous standard solutions with increasing NaCl concentrations, which served for the calibration of relative tissue Na^+ by a linear trend analysis.

Chemical Analysis of Murine Tissue Sodium. Tissue samples were carefully harvested in sodium-free tubes after perfusion with 5% glucose and freeze-dried with a Genesis 25EL freeze dryer (SP Scientific). Frozen samples were properly weighed into sodium-free quartz vessels and analyzed by inductively coupled plasma-optical emission spectroscopy after pressure digestion: First, 1 mL HNO3, Suprapur, subboiling distilled (Merck) was added. Subsequently, the vessels were closed and introduced into a pressure digestion system (Seif) for 10 h at 170 °C. The resulting clear solution was filled up to exactly 5 mL with Milli-Q water. An ICP-AES "Ciros Vision" system from SPECTRO Analytical Instruments GmbH & Co. KG was used for sodium and potassium determination in samples as described previously (48). The measured spectral element lines were K: 766.491 nm and Na: 589.592 nm. Calculation of results was carried out on a computerized laboratory data-management system relating the sample measurements to calibration curves, blank determinations, control standards, and the weight of the digested sample.

Statistical Analysis. Statistical analysis was performed using GraphPad Prism (GraphPad Software Inc.). All data were analyzed by one-way ANOVA followed by Tukey's posttest analysis and unpaired and paired t tests (unless indicated otherwise in the legends). Statistical analysis was corrected for multiple comparisons with the Bonferroni correction. Data are presented as mean ± SEM; $*P < 0.05$, $**P < 0.01$, or $***P < 0.001$ were considered to be statistically significant.

Data Availability. All study data are included in the article.

ACKNOWLEDGMENTS. We thank A. Hammer and K. Kuhbandner for helpful discussions and advice, as well as S. Seubert and K. Bitterer for expert technical assistance. Skin sodium imaging in mice was supported by the Preclinical Imaging Platform Erlangen (Friedrich–Alexander University Erlangen–Nuremberg, Germany). We thank the Imaging Science Institute (Erlangen, Germany) for providing us with measurement time at the 3-T MRI system. Jan Ruff improved the gradient echo sequence for ^{23}Na-MRI. We are grateful to Marc Schwarz for support in setting up murine magnetic resonance proton imaging.

1. M. Kleinewietfeld *et al*., Sodium chloride drives autoimmune disease by the induction of pathogenic TH17 cells. *Nature* **496**, 518–522 (2013).
2. C. Wu *et al*., Induction of pathogenic TH17 cells by inducible salt-sensing kinase SGK1. *Nature* **496**, 513–517 (2013).
3. S. Hucke *et al*., Sodium chloride promotes pro-inflammatory macrophage polarization thereby aggravating CNS autoimmunity. *J. Autoimmun.* **67**, 90–101 (2015).
4. W.-C. Zhang *et al*., High salt primes a specific activation state of macrophages, M(Na). *Cell Res.* **25**, 893–910 (2015).
5. D. N. Krementsov, L. K. Case, W. F. Hickey, C. Teuscher, Exacerbation of autoimmune neuroinflammation by dietary sodium is genetically controlled and sex specific. *FASEB J.* **29**, 3446–3457 (2015).
6. N. Ruggeri Barbaro *et al*., Sodium activates human monocytes via the NADPH oxidase and isolevuglandin formation. *Cardiovasc. Res.* **117**, 1358–1371 (2020).
7. M. F. Farez, M. P. Fiol, M. I. Gaitán, F. J. Quintana, J. Correale, Sodium intake is associated with increased disease activity in multiple sclerosis. *J. Neurol. Neurosurg. Psychiatry* **86**, 26–31 (2015).
8. K. C. Fitzgerald *et al*.; BENEFIT Study Group, Sodium intake and multiple sclerosis activity and progression in BENEFIT. *Ann. Neurol.* **82**, 20–29 (2017).
9. B. Nourbakhsh *et al*.; Network of Pediatric Multiple Sclerosis Centers, Dietary salt intake and time to relapse in paediatric multiple sclerosis. *J. Neurol. Neurosurg. Psychiatry* **87**, 1350–1353 (2016).
10. J. McDonald *et al*., A case-control study of dietary salt intake in pediatric-onset multiple sclerosis. *Mult. Scler. Relat. Disord.* **6**, 87–92 (2016).
11. M. Cortese, C. Yuan, T. Chitnis, A. Ascherio, K. L. Munger, No association between dietary sodium intake and the risk of multiple sclerosis. *Neurology* **89**, 1322–1329 (2017).
12. J. Titze, Sodium balance is not just a renal affair. *Curr. Opin. Nephrol. Hypertens.* **23**, 101–105 (2014).
13. M. Heer, F. Baisch, J. Kropp, R. Gerzer, C. Drummer, High dietary sodium chloride consumption may not induce body fluid retention in humans. *Am. J. Physiol. Renal Physiol.* **278**, F585–F595 (2000).
14. J. Titze *et al*., Long-term sodium balance in humans in a terrestrial space station simulation study. *Am. J. Kidney Dis.* **40**, 508–516 (2002).
15. M. Heer *et al*., Increasing sodium intake from a previous low or high intake affects water, electrolyte and acid-base balance differently. *Br. J. Nutr.* **101**, 1286–1294 (2009).
16. N. Rakova *et al*., Long-term space flight simulation reveals infradian rhythmicity in human Na(+) balance. *Cell Metab.* **17**, 125–131 (2013).
17. J. Titze *et al*., Glycosaminoglycan polymerization may enable osmotically inactive Na^+ storage in the skin. *Am. J. Physiol. Heart Circ. Physiol.* **287**, H203–H208 (2004).
18. H. Wiig *et al*., Immune cells control skin lymphatic electrolyte homeostasis and blood pressure. *J. Clin. Invest.* **123**, 2803–2815 (2013).
19. P. Linz *et al*., Skin sodium measured with ^{23}Na MRI at 7.0 T. *NMR Biomed.* **28**, 54–62 (2015).
20. H. Wiig, F. C. Luft, J. M. Titze, The interstitium conducts extrarenal storage of sodium and represents a third compartment essential for extracellular volume and blood pressure homeostasis. *Acta Physiol. (Oxf.)* **222**, e13006 (2018).
21. A. Machnik *et al*., Macrophages regulate salt-dependent volume and blood pressure by a vascular endothelial growth factor-C-dependent buffering mechanism. *Nat. Med.* **15**, 545–552 (2009).
22. C. Kopp *et al*., (23)Na magnetic resonance imaging of tissue sodium. *Hypertension* **59**, 167–172 (2012).
23. C. Kopp *et al*., ^{23}Na magnetic resonance imaging-determined tissue sodium in healthy subjects and hypertensive patients. *Hypertension* **61**, 635–640 (2013).
24. C. Kopp *et al*., Na^+ deposition in the fibrotic skin of systemic sclerosis patients detected by ^{23}Na-magnetic resonance imaging. *Rheumatology (Oxford)* **56**, 556–560 (2017).
25. J. Jantsch *et al*., Cutaneous Na^+ storage strengthens the antimicrobial barrier function of the skin and boosts macrophage-driven host defense. *Cell Metab.* **21**, 493–501 (2015).
26. C. Kopp *et al*., Elevated tissue sodium deposition in patients with type 2 diabetes on hemodialysis detected by ^{23}Na magnetic resonance imaging. *Kidney Int.* **93**, 1191–1197 (2018).
27. D. Kannenkeril *et al*., Tissue sodium content in patients with type 2 diabetes mellitus. *J. Diabetes Complications* **33**, 485–489 (2019).
28. D. A. Carranza-León *et al*., Tissue sodium content in patients with systemic lupus erythematosus: Association with disease activity and markers of inflammation. *Lupus* **29**, 455–462 (2020).
29. M. Hammon *et al*., ^{23}Na magnetic resonance imaging of the lower leg of acute heart failure patients during diuretic treatment. *PLoS One* **10**, e0141336 (2015).
30. M. Hammon *et al*., 3 Tesla ^{23}Na magnetic resonance imaging during acute kidney injury. *Acad. Radiol.* **24**, 1086–1093 (2017).

Downloaded at Palestinian Territory, occupied on November 29, 2021
www.manaraa.com

31. M. P. Schneider *et al*., Skin sodium concentration correlates with left ventricular hypertrophy in CKD. *J. Am. Soc. Nephrol.* **28**, 1867–1876 (2017).
32. E. Qirjazi *et al*., Tissue sodium concentrations in chronic kidney disease and dialysis patients by lower leg sodium-23 magnetic resonance imaging. *Nephrol. Dial. Transplant.* gfaa036 (2020).
33. W. Zaaraoui *et al*., Distribution of brain sodium accumulation correlates with disability in multiple sclerosis: A cross-sectional ^{23}Na MR imaging study. *Radiology* **264**, 859–867 (2012).
34. M. Petracca, L. Fleysher, N. Oesingmann, M. Inglese, Sodium MRI of multiple sclerosis. *NMR Biomed.* **29**, 153–161 (2016).
35. K. Huhn, T. Engelhorn, R. A. Linker, A. M. Nagel, Potential of sodium MRI as a biomarker for neurodegeneration and neuroinflammation in multiple sclerosis. *Front. Neurol.* **10**, 84 (2019).
36. P. Wang *et al*., Sex differences in sodium deposition in human muscle and skin. *Magn. Reson. Imaging* **36**, 93–97 (2017).
37. M. Sahinoz *et al*., Tissue sodium stores in peritoneal dialysis and hemodialysis patients determined by 23-sodium magnetic resonance imaging. *Nephrol. Dial. Transplant.* gfaa350 (2020).
38. C. Solaro *et al*., Prevalence of oedema of the lower limbs in multiple sclerosis patients: A vascular and lymphoscintigraphic study. *Mult. Scler.* **12**, 659–661 (2006).
39. L. Zhou *et al*., Validation of spot urine in predicting 24-h sodium excretion at the individual level. *Am. J. Clin. Nutr.* **105**, 1291–1296 (2017).
40. K. Lerchl *et al*., Agreement between 24-hour salt ingestion and sodium excretion in a controlled environment. *Hypertension* **66**, 850–857 (2015).
41. C. E. Dougher *et al*., Spot urine sodium measurements do not accurately estimate dietary sodium intake in chronic kidney disease. *Am. J. Clin. Nutr.* **104**, 298–305 (2016).
42. F. C. Luft, N. S. Fineberg, R. S. Sloan, Estimating dietary sodium intake in individuals receiving a randomly fluctuating intake. *Hypertension* **4**, 805–808 (1982).
43. G. Madelin, R. R. Regatte, Biomedical applications of sodium MRI in vivo. *J. Magn. Reson. Imaging* **38**, 511–529 (2013).
44. G. Madelin, J.-S. Lee, R. R. Regatte, A. Jerschow, Sodium MRI: Methods and applications. *Prog. Nucl. Magn. Reson. Spectrosc.* **79**, 14–47 (2014).
45. O. Zaric *et al*., Frontiers of sodium MRI revisited: From cartilage to brain imaging. *J. Magn. Reson. Imaging* **54**, 58–75 (2021).
46. K. J. Binger *et al*., High salt reduces the activation of IL-4- and IL-13-stimulated macrophages. *J. Clin. Invest.* **125**, 4223–4238 (2015).
47. S. Müller *et al*., Salt-dependent chemotaxis of macrophages. *PLoS One* **8**, e73439 (2013).
48. M. Fischereder *et al*., Sodium storage in human tissues is mediated by glycosaminoglycan expression. *Am. J. Physiol. Renal Physiol.* **313**, F319–F325 (2017).

Downloaded at Palestinian Territory, occupied on November 29, 2021

www.manaraa.com